COMMUNICATION

Check for updates

Electrochemical CO₂-to-CO *via* enriched oxygen vacancies at gold/ceria interfaces†

Zelun Zhao,‡[a] Chang Tan,‡[b] Peng Sun,[a] Fuwei Li*[ac] and Xue Wang [iD] *[b]

The carbon dioxide electroreduction reaction (CO₂RR) to carbon monoxide (CO) is a promising avenue to store renewable energy. Gold (Au) is a critical component of catalysts for CO production in the CO₂RR. Still, the high cost of Au together with the low mass activity hinders its potential towards practical CO₂RR application. Here we report a strategy of catalyst design, oxygen vacancy modulation *via* controlling Au/ceria interface structures, to promote Au mass activity for CO production ($j_{CO,mass}$) in the CO₂RR. Through ceria-nanocube-supported Au nanoparticle fabrication, we construct Au/CeO₂{100} interfaces with high concentration of oxygen vacancies facilitating CO₂ adsorption and activation. We achieve, at 200 mA cm⁻², a record $j_{CO,mass}$ of 678 mA mg$_{Au}$⁻¹ in the CO₂RR, a 1.3× improvement relative to the best prior reports.
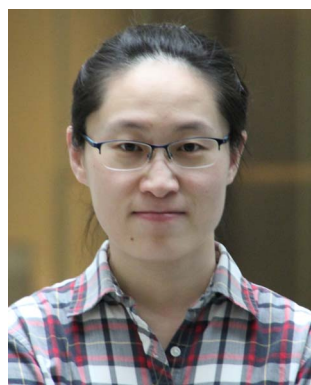
[a]State Key Laboratory of Low Carbon Catalysis and Carbon Dioxide Utilization, State Key Laboratory for Oxo Synthesis and Selective Oxidation, Lanzhou Institute of Chemical Physics, Chinese Academy of Sciences, Lanzhou, 730000, P. R. China. E-mail: fuweili@ucas.ac.cn

[b]School of Energy and Environment, State Key Laboratory of Marine Pollution, Department of Materials Science and Engineering, Hong Kong Institute for Clean Energy, City University of Hong Kong, Kowloon, Hong Kong. E-mail: xue.wang@cityu.edu.hk

[c]School of Chemical Engineering, University of Chinese Academy of Sciences, Beijing, 100049, P. R. China

‡ These authors contributed equally to this work.

Dr Xue Wang is currently an Assistant Professor at the School of Energy and Environment, City University of Hong Kong, where she joined the faculty in 2023. She received her PhD degree in physical chemistry from Xiamen University. During her graduate studies, she worked at the Georgia Institute of Technology as a visiting graduate student for two years. After her PhD graduation, she worked as an associate professor at the Lanzhou Institute of Chemical Physics, Chinese Academy of Sciences, and then as a postdoctoral fellow at the University of Toronto. Her research interests include nanomaterial design, CO₂ electrocatalysis and reaction engineering, as well as chemical/fuel electrosynthesis.

Xue Wang

Introduction

The CO₂ electroreduction reaction (CO₂RR) provides a promising avenue to store intermittent renewable energy in the form of feedstocks and chemicals.[1,2] Carbon monoxide (CO), the simplest carbonaceous product in the CO₂RR and a widely used feedstock to generate high-value added products, is of particular interest.[3–6] Gold (Au) nanoparticles are reported to be the most promising CO₂-to-CO electrocatalysts, theoretically ascribed to the optimal binding energy of the key intermediate carbon-bound *COOH for CO production on the Au surface.[7–11] However, the high cost of Au limits its potential practical application as a CO₂RR electrocatalyst.[12] In this regard, improving the mass activity of Au is highly desirable yet remains challenging.

The construction of a metal–oxide interface is a strategy to regulate the activity of the catalysts.[13–15] Bao *et al.* reported that Au–CeO$_x$ showed higher activity and CO selectivity compared to bare Au and CeO$_x$;[16] recent studies showed that Cu–BaO promoted CO₂-to-alcohol selectivity due to the interfacial Cu stabilizing hydroxy-containing intermediates.[17] These prior CO₂RR studies explored the effect of metal–oxide interfaces with different components on the performance. In addition, it is reported that metal nanoparticles loaded on oxide supports with different surface structures delivered different activities in heterogeneous catalysis such as the water gas shift reaction and steam reforming of methanol.[18,19] Taken together, we took the view that CO₂RR selectivity/activity would be promoted by controlling the structure of metal–oxide interfaces.

To validate this hypothesis, in this work, we used ceria-supported Au (Au/CeO₂) catalysts with different interfacial structures – Au/CeO₂{111}, Au/CeO₂{100}, and Au/CeO₂{110}

through loading Au nanoparticles onto ceria with different morphologies – as a model study for CO_2-to-CO electrolysis. Among all the Au/CeO_2 catalysts, ceria-nanocube-supported Au (Au/c-CeO_2) catalysts with the interface $Au/CeO_2\{100\}$ deliver the highest Faradaic efficiency (FE) of 89% towards CO in the CO_2RR, due to their abundant oxygen vacancies promoting CO_2 adsorption and activation. We have achieved a mass activity of 678 mA mg_{Au}^{-1} on Au/c-CeO_2 catalysts, a 1.3× improvement relative to the best prior reports (Table S1†).[4,20–23]

Results and discussion

To investigate the Au/CeO_2 interfacial effect on the CO_2RR, we sought to prepare ceria-supported Au catalysts with different interface structures. We first prepared three types of CeO_2 with different morphologies (Fig. S1 and S2†) – including rods enclosed by $\{110\}$ and $\{100\}$ facets, cubes enclosed by $\{100\}$ facets, and octahedra enclosed by $\{111\}$ facets (denoted as r-CeO_2, c-CeO_2, and o-CeO_2, respectively) – using modified hydrothermal protocols reported previously (see the ESI†).[24,25] We then prepared Au/CeO_2 using a modified deposition–precipitation method.[26] $HAuCl_4$ aqueous solution was added dropwise to the CeO_2 slurry solution, followed by adding aqueous ammonia slowly. The mixture was then kept in a water bath at 60 °C for 4 hours with constant stirring. The collected light-yellow precipitates were further calcined at 200 °C for 1 hour in air and then we obtained Au–CeO_2 catalysts (Fig. 1).
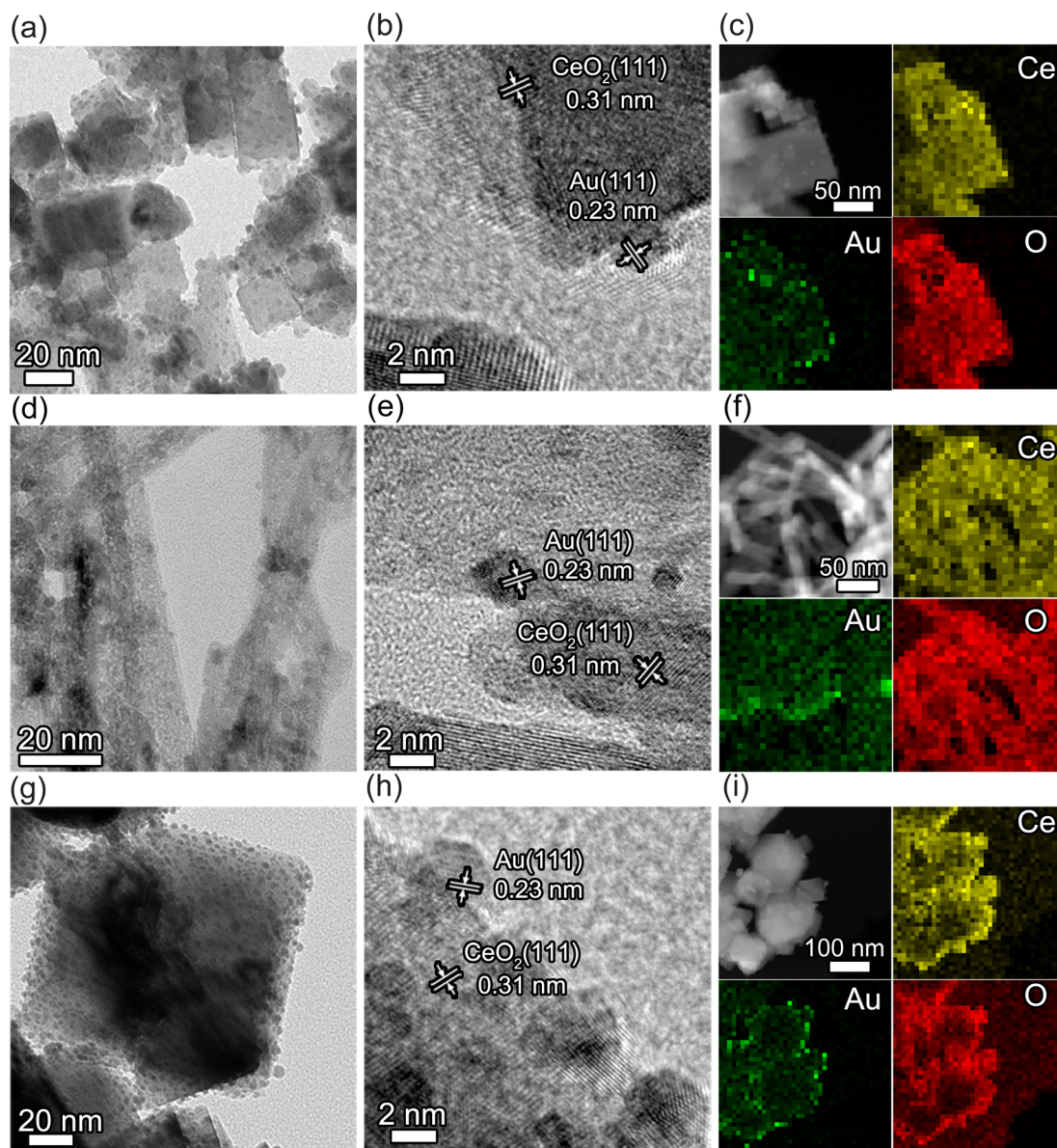

Fig. 1 (a and b) TEM and HRTEM images of Au/c-CeO_2 catalysts. (c) High-angle annular dark-field scanning transmission electron microscopy (HAADF-STEM) image of Au/c-CeO_2 catalysts and the corresponding EDX elemental mapping of Ce, Au, and O. (d and e) TEM and HRTEM images of Au/r-CeO_2 catalysts. (f) HAADF-STEM image of Au/r-CeO_2 catalysts and the corresponding EDX elemental mapping of Ce, Au, and O. (g and h) TEM and HRTEM images of Au/o-CeO_2 catalysts. (i) HAADF-STEM image of Au/o-CeO_2 catalysts and the corresponding EDX elemental mapping of Ce, Au, and O.

This journal is © The Royal Society of Chemistry 2024

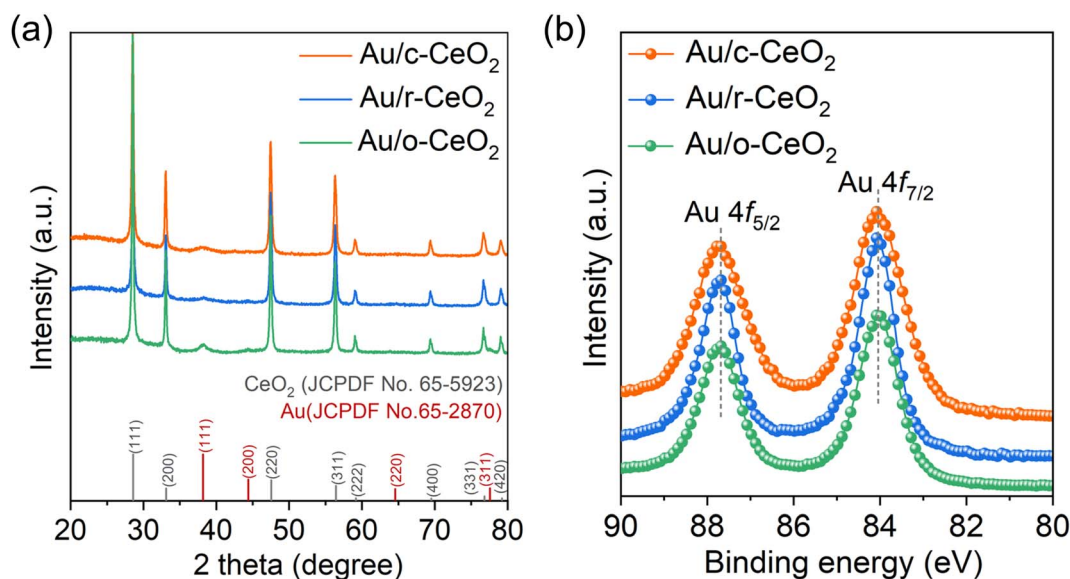*J. Mater. Chem. A*, 2024, **12**, 21716–21722 | **21717**

Fig. 2 (a) XRD patterns of Au/CeO$_2$ catalysts. (b) Au 4f XPS spectra of Au/CeO$_2$ catalysts.

The transmission electron microscope (TEM) images of three different Au–CeO$_2$ catalysts and their energy-dispersive X-ray spectroscopy (EDX) elemental mapping of Au, Ce, and O show Au nanoparticles distributed evenly on the surfaces of c-CeO$_2$, r-CeO$_2$, and o-CeO$_2$ (Fig. 1), generating interface structures of Au/CeO$_2${100}, Au/CeO$_2${110}, and Au/CeO$_2${111}. The lattice spacings of 0.23 and 0.31 nm in high-resolution transmission electron microscope (HRTEM) images correspond to the (111) lattice plane of Au and the (111) lattice plane of CeO$_2$, respectively (Fig. 1b). The average sizes of Au nanoparticles on CeO$_2$ cubes, rods, and octahedra are close to each other, corresponding to 2.4, 2.3, and 2.8 nm, respectively (Fig. S3†). The powder X-ray diffraction (XRD) results further demonstrate the existence of CeO$_2$ and Au in the as-prepared catalysts (Fig. 2a). X-ray photoelectron spectroscopy (XPS) confirms that Au nanoparticles in the as-prepared Au/c-CeO$_2$, Au/r-CeO$_2$, and Au/o-CeO$_2$ catalysts are in the metallic state (Fig. 2b). On the basis of inductively coupled plasma mass spectrometry (ICP-MS) analysis, the weight percentage (wt%) of Au in the three as-prepared Au/CeO$_2$ catalysts are similar, 7.8 wt%, 8.1 wt%, and 7.9 wt% for Au/c-CeO$_2$, Au/r-CeO$_2$, and Au/o-CeO$_2$, respectively. N 1s XPS spectra show that there is no N element in Au/c-CeO$_2$, Au/r-CeO$_2$, and Au/o-CeO$_2$ catalysts after annealing treatment (Fig. S4†).

We then investigated the CO$_2$RR performance of Au/c-CeO$_2$, Au/r-CeO$_2$, and Au/o-CeO$_2$ catalysts in a flow cell reactor (Fig. 3 and Table S2†). The cathodes were prepared by depositing Au/CeO$_2$ nanocatalysts onto a carbon-based gas diffusion layer (GDL) using spray-coating to get gas diffusion electrodes (GDEs). Only the products H$_2$, CO, and formate were detected on Au/CeO$_2$ catalysts in the CO$_2$RR (Fig. 3 and Table S2†). Fig. 3a–c show FEs of gas products quantified using gas chromatography on different Au/CeO$_2$ catalysts as a function of total current densities using 1 M KOH electrolyte in the CO$_2$RR. The main carbonaceous product during the CO$_2$RR on Au/CeO$_2$

catalysts is CO. CO FEs on different electrodes follow the sequence Au/c-CeO$_2$ > Au/r-CeO$_2$ > Au/o-CeO$_2$. The highest CO FE on Au/c-CeO$_2$ catalysts is 89% at 50 mA cm^{-2}. At an industrially relevant current density of 100 mA cm^{-2}, Au/c-CeO$_2$ catalysts deliver a CO FE of 78% (Fig. 3a). We further normalized the partial CO current density by using Au mass to obtain mass activity for CO production ($j_{CO,mass}$) in the CO$_2$RR (Fig. 3d). The $j_{CO,mass}$ on Au/c-CeO$_2$ is higher than those on Au/r-CeO$_2$ and Au/o-CeO$_2$, respectively, suggesting that the interface Au/CeO$_2${100} promotes the CO selectivity in the CO$_2$RR. At 200 mA cm^{-2}, the $j_{CO,mass}$ on Au/c-CeO$_2$ reaches 678 mA mg$_{Au}^{-1}$ – representing a 1.3× improvement compared to the best value reported (Table S1†). The liquid product formate following the CO$_2$RR was also detected and all the Au/CeO$_2$ catalysts deliver similar formate FEs of 2–4% quantified by high-performance liquid chromatography (HPLC) in the current density range of 50–200 mA cm^{-2} (Table S2†).

As controls, we also prepared gas diffusion electrodes of c-CeO$_2$, r-CeO$_2$, and o-CeO$_2$ using spray-coating and measured their CO$_2$RR performance in the range of 50–200 mA cm^{-2} (Fig. S5 and Table S3†). The c-CeO$_2$, r-CeO$_2$, and o-CeO$_2$ catalysts deliver CO with a FE below 10% – much lower than that of Au/c-CeO$_2$, Au/r-CeO$_2$, and Au/o-CeO$_2$ catalysts – and the competing hydrogen evolution reaction (HER) is dominant with a H$_2$ FE above 86%, suggesting that the Au–CeO$_2$ interface rather than CeO$_2$ is the active site for CO$_2$ electroreduction and Au/CeO$_2$ catalysts with different Au–CeO$_2$ interface structures prompt different CO selectivities in the CO$_2$RR.

To investigate the surface/interface structure of Au/c-CeO$_2$, Au/r-CeO$_2$, and Au/o-CeO$_2$ catalysts, we performed XPS measurements. As shown in Fig. 3a–c, the Ce 3d XPS spectra are deconvoluted into two groups of peaks, demonstrating the mixture of Ce^{4+} and Ce^{3+} in Au/c-CeO$_2$, Au/r-CeO$_2$, and Au/o-CeO$_2$ catalysts.[27] The Ce^{3+} atomic fractions – determined by fitting Ce 3d peaks – in Au/c-CeO$_2$, Au/r-CeO$_2$, and Au/o-CeO$_2$

21718 | J. Mater. Chem. A, 2024, 12, 21716–21722

This journal is © The Royal Society of Chemistry 2024
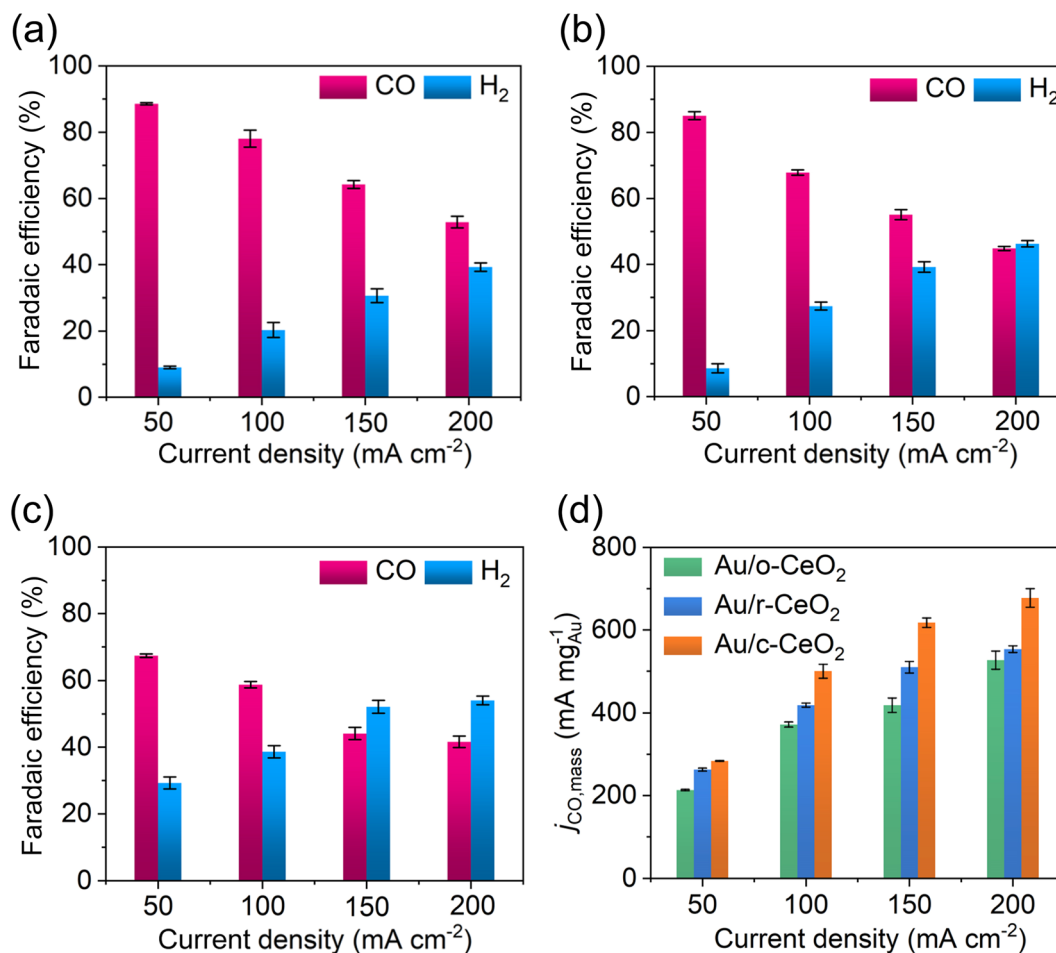
Fig. 3 CO_2RR gas product distribution on (a) Au/c-CeO_2, (b) Au/r-CeO_2, and (c) Au/o-CeO_2 GDEs. (d) Mass activity for CO production on different Au/CeO_2 GDEs. Error bars refer to the standard deviation based on the three repeated experiments.

catalysts are 33%, 29%, and 24%, respectively. Compared to Au/r-CeO_2 and Au/o-CeO_2 catalysts, a higher ratio of Ce^{3+} in Au/c-CeO_2 catalysts indicates higher concentration of oxygen vacancy defects.[16,28]

To quantify oxygen vacancy defects of different Au/CeO_2 catalysts, we analyzed O 1s XPS spectra of the catalysts. For every sample, each O 1s XPS spectrum can be decomposed into three Gaussian components centered at 529.1, 530.9, and 532.5 eV (Fig. 3d) after Gaussian fitting, corresponding to lattice oxygen (O_L) of CeO_2, the oxygen species associated with oxygen vacancies (O_V) within the CeO_2 matrix, and chemisorbed and dissociated oxygen species or OH (O_C), respectively.[29] The O_L, O_V, and O_C components of O 1s spectra are associated with O^{2-} ions in the CeO_2 lattices, oxygen vacancy defects within the CeO_2 matrix, and chemisorbed and dissociated oxygen species or OH, respectively.[29] The O_V components of different catalysts follow the sequence Au/c-CeO_2 (30%) > Au/r-CeO_2 (26%) > Au/o-CeO_2 (23%). As controls, we also carried out XPS measurements on different CeO_2 catalysts (Fig. S6†). The analysis of the O 1s XPS spectra of CeO_2 catalysts shows that the density of O_V decreases in the order of c-CeO_2 (20%), r-CeO_2 (16%), and o-CeO_2 (15%), indicating that the density of O_V is associated with facet

exposure of CeO_2. The introduction of Au onto CeO_2 catalysts further increases O_V densities (Fig. 4 and S6†), arising from the interaction between Au and CeO_2.[30–35]

To probe the oxygen vacancies further among different catalysts, we also carried out ultraviolet (UV) Raman spectroscopy measurement. As shown in Fig. 5, two main peaks are observed in the Au/CeO_2 spectra in the region of 300–800 cm^{-1}. The strong F_{2g} vibrational peak located at ~458 cm^{-1} is ascribed to the symmetric stretching mode of the Ce–O8 crystal unit and the vibrational peak at ~594 cm^{-1} is associated with oxygen vacancy defects (D mode).[36] The oxygen vacancy concentrations of CeO_2 in Au–CeO_2 catalysts are estimated through the calculation of integrating peak area ratios (I_D/F_{2g}).[37] The I_D/I_{F2g} values of Au/c-CeO_2, Au/r-CeO_2, and Au/o-CeO_2 catalysts are 0.55, 0.32, and 0.17, respectively, suggesting that the oxygen vacancy concentrations of the catalysts increase in the order of Au/o-CeO_2, Au/r-CeO_2, and Au/c-CeO_2, consistent with XPS analysis results. We also measured UV Raman spectra of o-CeO_2, r-CeO_2, and c-CeO_2 catalysts as controls (Fig. S7†). We find that, at ~594 cm^{-1}, all the CeO_2 catalysts do not have obvious peaks while Au/CeO_2 catalysts have peaks, indicating that the increase in oxygen vacancies on Au/CeO_2 catalysts is induced by the
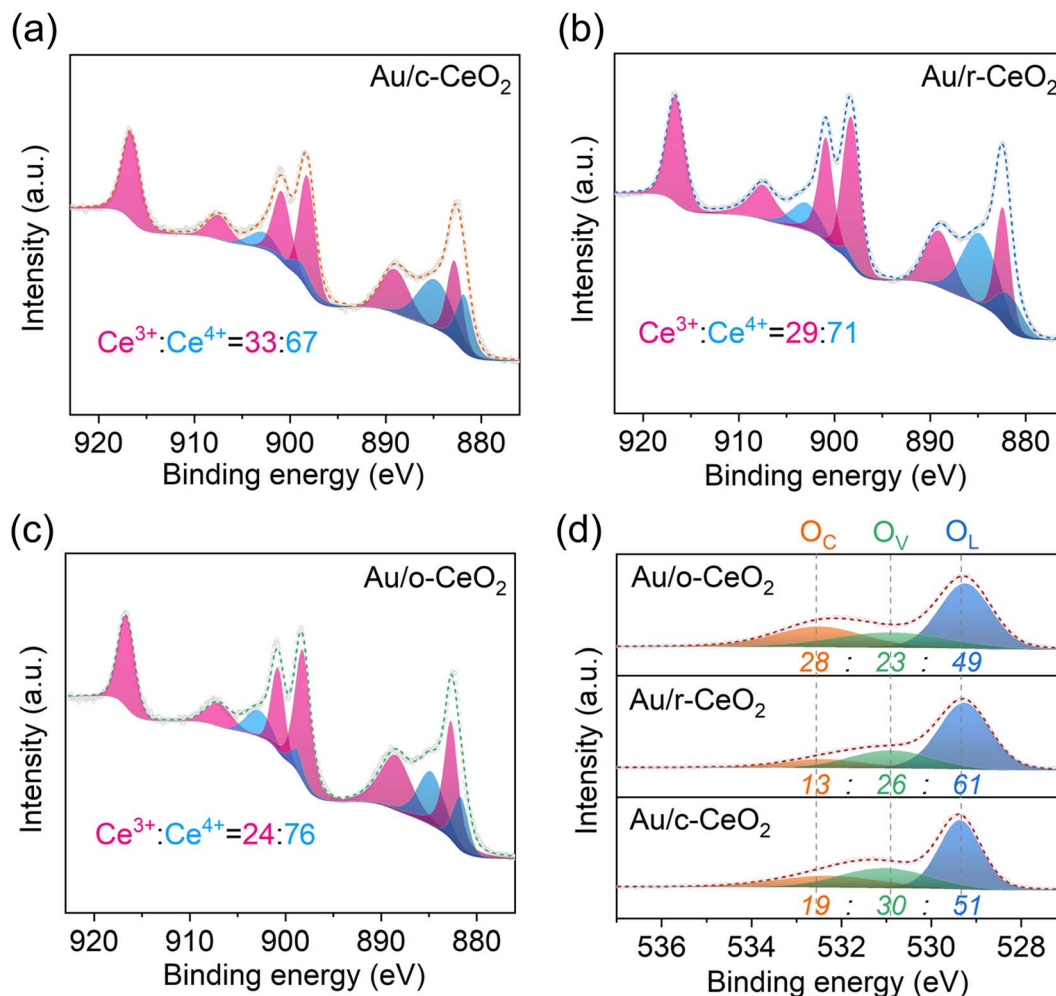
This journal is © The Royal Society of Chemistry 2024

J. Mater. Chem. A, 2024, **12**, 21716–21722 | **21719**

Fig. 4 Ce 3d XPS spectra of (a) Au/c-CeO$_2$, (b) Au/r-CeO$_2$, and (c) Au/o-CeO$_2$ catalysts. (d) O 1s XPS spectra of Au/CeO$_2$ catalysts.
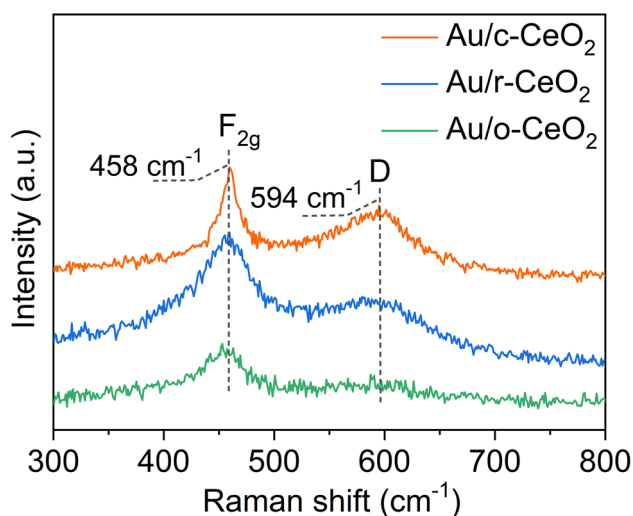

Fig. 5 UV Raman spectra of Au/CeO$_2$ catalysts.

construction of Au/CeO$_2$ interface structures. Thus, we conclude that the concentrations of O$_V$ induced by the interaction between Au and CeO$_2$ are modulated through the construction

of different Au–CeO$_2$ interface structures. Prior studies showed that the O$_V$ induced by the metal–oxide interaction could promote CO$_2$ adsorption and activation for the key intermediate *COOH generation in CO$_2$-to-CO electrolysis.[38] Among Au/o-CeO$_2$, Au/r-CeO$_2$, and Au/c-CeO$_2$ catalysts, Au/c-CeO$_2$ catalysts with Au/CeO$_2${100} interfaces show the highest concentration of O$_V$ induced by the Au–CeO$_2$ interaction, thereby facilitating CO$_2$ adsorption and activation, thus promoting CO$_2$ electroreduction.

Conclusions

In summary, we have fabricated three types of Au/CeO$_2$ catalysts with different interface structures and have investigated the Au/CeO$_2$ interfacial effect on the CO$_2$RR. Compared to Au/r-CeO$_2$ and Au/o-CeO$_2$ catalysts, the Au/c-CeO$_2$ catalyst with the interface Au/CeO$_2${111} exhibited the highest CO FE of 89% in the CO$_2$RR. The enhanced CO selectivity on the Au/c-CeO$_2$ catalyst is ascribed to the increase in oxygen vacancies – resulting from the interface structure of Au/CeO$_2${111} – which facilitates CO$_2$ adsorption and activation in the CO$_2$RR. Specifically, at an industrially relevant current density of 200 mA cm^{-2}, we achieve

a mass activity of 678 mA mg_{Au}^{-1} for CO production. This work paves a way to improve the selectivity and activity in the CO_2RR by design and control of metal–oxide interface structures.

Data availability

The data supporting this article have been included as part of the ESI.†

Author contributions

X. W. supervised the project, conceived the idea, and designed the experiments. Z. Z. prepared the catalysts and performed the structure analysis. C. T. performed CO_2RR measurements and analyzed the results. X. W. and Z. Z. co-wrote the manuscript. P. S., and F. L. discussed the results and assisted during the manuscript preparation.

Conflicts of interest

There are no conflicts of interest.

Acknowledgements

References

1 N. Mac Dowell, P. S. Fennell, N. Shah and G. C. Maitland, *Nat. Clim. Change*, 2017, **7**, 243–249.

2 J. Artz, T. E. Müller, K. Thenert, J. Kleinekorte, R. Meys, A. Sternberg, A. Bardow and W. Leitner, *Chem. Rev.*, 2018, **118**, 434–504.

3 S. Ren, D. Joulié, D. Salvatore, K. Torbensen, M. Wang, M. Robert and C. P. Berlinguette, *Science*, 2019, **365**, 367–369.

4 M. C. O. Monteiro, M. F. Philips, K. J. P. Schouten and M. T. M. Koper, *Nat. Commun.*, 2021, **12**, 4943.

5 W. Zhu, Y.-J. Zhang, H. Zhang, H. Lv, Q. Li, R. Michalsky, A. A. Peterson and S. Sun, *J. Am. Chem. Soc.*, 2014, **136**, 16132–16135.

6 H. Mistry, R. Reske, Z. Zeng, Z.-J. Zhao, J. Greeley, P. Strasser and B. Roldan Cuenya, *J. Am. Chem. Soc.*, 2014, **136**, 16473–16476.

7 J. T. Feaster, C. Shi, E. R. Cave, T. Hatsukade, D. N. Abram, K. P. Kuhl, C. Hahn, J. K. Nørskov and T. F. Jaramillo, *ACS Catal.*, 2017, **7**, 4822–4827.

8 M. Sassenburg, R. de Rooij, N. T. Nesbitt, R. Kas, S. Chandrashekar, N. J. Firet, K. Yang, K. Liu, M. A. Blommaert, M. Kolen, D. Ripepi, W. A. Smith and T. Burdyny, *ACS Appl. Energy Mater.*, 2022, **5**, 5983–5994.

9 A. Q. Fenwick, A. J. Welch, X. Li, I. Sullivan, J. S. DuChene, C. Xiang and H. A. Atwater, *ACS Energy Lett.*, 2022, **7**, 871–879.

10 K. Sun, Y. Shi, H. Li, J. Shan, C. Sun, Z.-Y. Wu, Y. Ji and Z. Wang, *ChemSusChem*, 2021, **14**, 4929–4935.

11 S. Gao, M. Jin, J. Sun, X. Liu, S. Zhang, H. Li, J. Luo and X. Sun, *J. Mater. Chem. A*, 2021, **9**, 21024–21031.

12 K. C. Poon, W. Y. Wan, H. Su and H. Sato, *RSC Adv.*, 2022, **12**, 22703–22721.

13 F. Yang, D. Deng, X. Pan, Q. Fu and X. Bao, *Natl. Sci. Rev.*, 2015, **2**, 183–201.

14 R. Si and M. Flytzani-Stephanopoulos, *Angew. Chem., Int. Ed.*, 2008, **47**, 2884–2887.

15 X. Wang, J. Chen, J. Zeng, Q. Wang, Z. Li, R. Qin, C. Wu, Z. Xie and L. Zheng, *Nanoscale*, 2017, **9**, 6643–6648.

16 D. Gao, Y. Zhang, Z. Zhou, F. Cai, X. Zhao, W. Huang, Y. Li, J. Zhu, P. Liu, F. Yang, G. Wang and X. Bao, *J. Am. Chem. Soc.*, 2017, **139**, 5652–5655.

17 A. Xu, S.-F. Hung, A. Cao, Z. Wang, N. Karmodak, J. E. Huang, Y. Yan, A. Sedighian Rasouli, A. Ozden, F.-Y. Wu, Z.-Y. Lin, H.-J. Tsai, T.-J. Lee, F. Li, M. Luo, Y. Wang, X. Wang, J. Abed, Z. Wang, D.-H. Nam, Y. C. Li, A. H. Ip, D. Sinton, C. Dong and E. H. Sargent, *Nat. Catal.*, 2022, **5**, 1081–1088.

18 M. B. Boucher, S. Goergen, N. Yi and M. Flytzani-Stephanopoulos, *Phys. Chem. Chem. Phys.*, 2011, **13**, 2517–2527.

19 N. Yi, R. Si, H. Saltsburg and M. Flytzani-Stephanopoulos, *Energy Environ. Sci.*, 2010, **3**, 831–837.

20 P. Zhan, S. Yang, L. Huang, X. Zhang, X. Li, L. Lu and P. Qin, *Langmuir*, 2023, **39**, 8306–8313.

21 J. Wang, J. Yu, M. Sun, L. Liao, Q. Zhang, L. Zhai, X. Zhou, L. Li, G. Wang, F. Meng, D. Shen, Z. Li, H. Bao, Y. Wang, J. Zhou, Y. Chen, W. Niu, B. Huang, L. Gu, C.-S. Lee and Z. Fan, *Small*, 2022, **18**, 2106766.

22 J. W. Park, W. Choi, J. Noh, W. Park, G. H. Gu, J. Park, Y. Jung and H. Song, *ACS Appl. Mater. Interfaces*, 2022, **14**, 6604–6614.

23 L.-W. Chen, Y.-C. Hao, J. Li, L. Hu, Y. Guo, S. Li, D. Liu, Z. Zhu, S.-Q. Wu, H.-Z. Huang, A.-X. Yin, B. Wang and Y.-W. Zhang, *Sci. China: Chem.*, 2022, **65**, 2188–2196.

24 H.-X. Mai, L.-D. Sun, Y.-W. Zhang, R. Si, W. Feng, H.-P. Zhang, H.-C. Liu and C.-H. Yan, *J. Phys. Chem. B*, 2005, **109**, 24380–24385.

25 L. Yan, R. Yu, J. Chen and X. Xing, *Cryst. Growth Des.*, 2008, **8**, 1474–1477.

26 J. Zhang, X. Liu, S. Wu, M. Xu, X. Guo and S. Wang, *J. Mater. Chem.*, 2010, **20**, 6453–6459.

27 A. Chen, X. Yu, Y. Zhou, S. Miao, Y. Li, S. Kuld, J. Sehested, J. Liu, T. Aoki, S. Hong, M. Farnesi Camellone, S. Fabris, J. Ning, C. Jin, C. Yang, A. Nefedov, C. Wöll, Y. Wang and W. Shen, *Nat. Catal.*, 2019, **2**, 334–341.

28 F. Esch, S. Fabris, L. Zhou, T. Montini, C. Africh, P. Fornasiero, G. Comelli and R. Rosei, *Science*, 2005, **309**, 752–755.

29 X. Wang, Z. Jiang, B. Zheng, Z. Xie and L. Zheng, *CrystEngComm*, 2012, **14**, 7579–7582.

This journal is © The Royal Society of Chemistry 2024

J. Mater. Chem. A, 2024, **12**, 21716–21722 | **21721**

30 F. Jiang, S. Wang, B. Liu, J. Liu, L. Wang, Y. Xiao, Y. Xu and X. Liu, *ACS Catal.*, 2020, **10**, 11493–11509.

31 S. Chen, S. Li, R. You, Z. Guo, F. Wang, G. Li, W. Yuan, B. Zhu, Y. Gao, Z. Zhang, H. Yang and Y. Wang, *ACS Catal.*, 2021, **11**, 5666–5677.

32 A. Chutia, D. J. Willock and C. R. A. Catlow, *Faraday Discuss.*, 2018, **208**, 123–145.

33 K.-J. Zhu, Y.-J. Yang, J.-J. Lang, B.-T. Teng, F.-M. Wu, S.-Y. Du and X.-D. Wen, *Appl. Surf. Sci.*, 2016, **387**, 557–568.

34 M. Nolan, *J. Chem. Phys.*, 2012, **136**, 13470.

35 S. Chang, M. Li, Q. Hua, L. Zhang, Y. Ma, B. Ye and W. Huang, *J. Catal.*, 2012, **293**, 195–204.

36 E. Sartoretti, C. Novara, F. Giorgis, M. Piumetti, S. Bensaid, N. Russo and D. Fino, *Sci. Rep.*, 2019, **9**, 3875.

37 X. Zhang, R. You, D. Li, T. Cao and W. Huang, *ACS Appl. Mater. Interfaces*, 2017, **9**, 35897–35907.

38 Y. Liang, C. Wu, S. Meng, Z. Lu, R. Zhao, H. Wang, Z. Liu and J. Wang, *ACS Appl. Mater. Interfaces*, 2023, **15**, 30262–30271.